ADVANCED OPTICAL MATERIALS
www.advopticalmat.de

Silk Foam Terahertz Waveguides

*Hichem Guerboukha, Guofeng Yan, Olga Skorobogata, and Maksim Skorobogatiy**

Fabrication and characterization in the THz frequency range of silk foams and silk foam-based waveguides using lyophilisation and casting techniques are reported. The lack of biocompatible and biofriendly waveguides for low-loss, low-dispersion guidance of THz waves motivates the work for applications in remote and stand-off sensing in biomedical and agro-alimentary industries. Silk foams produced are 94% porous. Optical characterization is carried out using THz time-domain spectroscopy. The cutback measurements of foam samples show that the foam refractive index is close to that of air ($n^r_{foam} \approx 1.06$). Silk foam losses scale quadratically with frequency ($\alpha_{foam}\left[cm^{-1}\right] \approx 0.65 + 2.75 \cdot \left(\nu\left[THz\right]\right)^2$), being one order of magnitude smaller than those of solid silk. As an example of a basic guided wave device, fabrication and optical characterization of 10 cm-long, 5 mm-diameter step-index THz fibers having silk foam in the core and air in the cladding is demonstrated. Cutback measurements confirm that in the mid-THz spectral range, step-index fibers operate effectively in a single mode regime. Effective refractive index and propagation loss at frequencies higher that 0.2 THz are close to that of a silk foam from which the fiber core is made. At the same time, at these frequencies, modal group velocity dispersion is smaller than $0.2 ps/(THz \cdot cm)$.

1. Introduction

Silk is a unique kind of nature protein derived from spiders or worms and it is the strongest natural fiber known to man.[1] Bombyx mori silk has excellent mechanical properties, smooth texture and shimmering appearance, so it has been widely used in textile industry over the past five millennia, since its first appearance in Imperial China.[2,3] Owing to its excellent mechanical and optical properties,[4–7] biocompatibility, biodegradability[8,9] and implant ability,[10–12] in recent years, this ancient material has been introduced into biomedical field as a promising biomaterial which opened a new era in the development of optical interfaces and sensors for biomedical applications. Silk material from worm cocoon can be processed into different forms, such as spheres, sponges, fibers,[13–15] foams[16] and films.[4,9,11,12] Among these various forms, silk films attracted significant attention for applications in optics and photonics, due to high transparency (>95%) and excellent surface flatness of such films. As a result, a great variety of optical devices has been fabricated using silk films. For example, silk-based diffractive gratings have been fabricated by casting silk solution onto polydimethylsiloxane (PDMS) negative molds. Silk lenses, microlens arrays and 64-phase level 2D diffraction masks were realized using molding technique.[4,17] Doped fluorescent silk-protein films with a two-dimensional square lattice of air holes were proposed and demonstrated to achieve enhancement in fluorescent emission.[18] Active optical optofluidic pH sensor were realized by chemical modification of the silk protein films with 4-aminobenzoic and by combining the elastomer in a single microfluidic device.[19]

Although many silk-based optical devices have been demonstrated, most of them operate in the visible region.[4,5,11,17–19] Recently, the growing demand for THz waveguides and sensors for non-destructive sensing in biomedicine and agriculture is motivating silk material research in THz region. In 2010, split ring resonator-based metamaterials using silk films as a substrate were demonstrated.[20] The authors also showed that silk is semi-transparent in the 0.15–1.5 THz region, having a relatively high loss of ~15 cm^{-1} at 0.3 THz. In 2012, the same group demonstrated conformal, adhesive, edible food sensors[21] based on the THz metamaterials on silk substrates. By monitoring the antenna resonant response that changes continuously during the food storage, the authors have demonstrated potential of this technology for monitoring changes in the food quality.

To the best of our knowledge, up to date, there were no reports of using silk to fabricate THz waveguides. This, most probably, is related to the high absorption loss of silk in the THz spectral region. Indeed, bulk absorption loss of silk is almost hundred times larger than the bulk absorption loss of polyethylene (~0.2 cm^{-1} at 0.3 THz), which is often used for fabrication of THz fibers.[22–24] At the same time, low-loss, low-dispersion waveguides for delivery of THz light is an important

H. Guerboukha, Dr. M. Skorobogatiy
Department of Engineering Physics
Ecole Polytechnique de Montréal
H3C 3A7, Montreal, Quebec, Canada
E-mail: maksim.skorobogatiy@polymtl.ca
G. Yan
Centre for Optical and Electromagnetic Research
State Key Laboratory of Modern Optical Instrumentation
Zhejiang University
Hangzhou 310058, China
O. Skorobogata
Department of Anatomy and Cell Biology
McGill University
H3A 0G4, Montréal, Québec, Canada

DOI: 10.1002/adom.201400228

enabling technology for stand-off and remote detection using THz waves. Additionally, in biomedical applications, it is desirable to interface THz waveguides directly with the living tissues, which requires the waveguide material to be biocompatible. Hence, using biocompatible materials to guide THz waves can be of significant interest for stand-off and remote sensing in bio-medical, agro-alimentary and other industries.

We note that for applications in the visible spectral range,[5] direct writing of silk-based waveguides was recently demonstrated by extrusion of highly concentrated silk solution (~28–30 wt%) through a 5 μm glass deposition nozzle into a methanol-rich reservoir. Unfortunately, this extrusion method cannot be used directly to produce THz fibers as it results in solid core waveguides that show very high absorption loss in THz spectral region. Moreover, extrusion of silk waveguides from aqueous solution can present additional challenge for THz applications due to residual concentration of highly absorbing water molecules in such waveguides.

An alternative fabrication strategy for silk fibers is a direct drawing from a macroscopic preform in a draw tower. Unfortunately, despite the fact that Bombyx mori silk has glass transition temperature ~ 175 °C and crystallization temperature ~212 °C, when heated at a relatively slow rate like 1–20 K/min, the silk melting transition will be obscured by decomposition.[25] It is reported in[26] that at a slow heat rate of 2 K/min the thermal decomposition begins at ~200 °C, and continues over a broad temperature range, causing mass loss and charring.

The lowest loss materials for THz propagation are dry gases. Therefore, one of the ways to reduce absorption loss is to maximize the fraction of light guided in the gas phase. Foams are inherently highly porous materials featuring both solid and gaseous phases. Polymer foams are used in the industry for various applications including packaging, thermal, acoustic insulation etc. Polystyrene foam was studied at THz frequencies.[27,28] Very low refractive indices of 1.017–1.022 in the 0.1–4 THz spectral range were found as well as a small extinction coefficient (smaller than 1.5 cm^{-1} below 4 THz). Polymethacrylimide foam showed the same kind of behavior at THz frequencies.[29] A typical way to produce polystyrene foam is to use pentane gas as a blowing agent to expand the polystyrene beads until they take the shape of a mold. We believe that foam synthesis within a mold is an interesting alternative to fiber drawing technique that is normally used to produce fibers from thermoplastics and glasses. As foam fabrication is not limited to thermoelastic materials, it, thus, opens new possibilities for development of optical waveguides from advanced materials.

In this paper, we have developed a fabrication method that uses casting from aqueous silk solution in order to produce silk foams through lyophilisation technique. To our knowledge, this is the first time when silk-based waveguides with sub 1 cm^{-1} losses are demonstrated in the mid-THz frequency range. The paper is organized as follows. Section 2 presents characterization of the bulk optical properties of silk foams. Section 3 describes characterization of the optical properties of THz silk-foam fibers. Section 4 presents numerical simulations that detail guidance properties of the silk-foam fibers including propagation loss and modal dispersion. Finally, a detailed comparison between numerical and experimental results is presented.

2. Characterization of Silk Foams

2.1. Characterization of Silk Foam Porosity

In **Figure 1**(a) we present picture of a typical sample of silk foam cast in a conical test tube. Characterization of the foam porosity and its uniformity along the sample length was carried out using cutback technique. Within this method one performs a series of straight cuts through the cylindrical portion of a sample (see **Table 1**). As each cut section has a simple cylindrical shape, its volume ΔV can be readily evaluated. After each cut, we re-measure the diameter D_2, the length L, and the weight of the remaining foam sample (see Table 1). From these measurements, and using the value of $\rho_f = 1.35$ g/cm^3 for the density of silk fibroin,[30] the local filling factor of the cut piece can be evaluated as $V_{fibroin}/V_{sample} = \Delta m/(\Delta V \cdot \rho_f)$, where Δm is the mass of a cut section. As shown in Table 1 the silk fibroin filling factor is low ~5–6%, and slow varying along the sample length, while corresponding porosity (air fraction by volume) of the fabricated foams is higher than 94%.

Moreover, when looking at the silk foam sample crossection (see Figure 1(b)) we notice highly symmetric patterns formed by the domains of crystallized silk fibroin. Those domains have needle-like shapes extending from the sample center towards the sample periphery. They are multicolored and they shimmer under white light illumination, suggesting thin-film optical interference effects due to silk foam microstructure. Scanning electron microscopy images of the sample crossection (Figure 1(c–f)) reveal an intricate flaky structure of the silk foams. Namely, the crystallized silk fibroin form crumpled stacks of thin layers that are generally extending from the sample center towards the periphery. The individual silk layers are ~2 μm thick and there is 30–50 μm separation between layers. Additionally, one notices small 1–5 μm diameter pores piercing the silk layers.

We believe that the radial pattern in Figure 1 is caused by the directional dynamics of the freezing process, as well as circular shape of the container. In principal, controlled freezing in judicially shaped containers could lead to designer microstructure alignment that would impact both terahertz wave propagation and its polarization properties.

2.2. Optical Characterization of Silk Foams in the THz Spectral Range

In order to obtain complex refractive index of silk foams, we used THz Time-Domain Spectroscopy (THz-TDS) setup described in ref. [31]. Cutback measurements were performed using conical shaped samples (see Figure 1) as obtained directly from the lyophilisation setup. During individual measurements, the small facet of each sample was placed against a semi-closed 3 mm-diameter aperture (A1, **Figure 2**), while the larger diameter end of the sample was placed against an open aperture (A2, Figure 2). To ensure consistent measurement conditions, the iris with 3 mm opening was placed at the focal point of a focusing parabolic mirror. The iris was placed on a 3D stage and aligned with the center of the focused beam. The second parabolic mirror (PM2) of 10 cm focal distance

Adv. Optical Mater. 2014,
DOI: 10.1002/adom.201400228

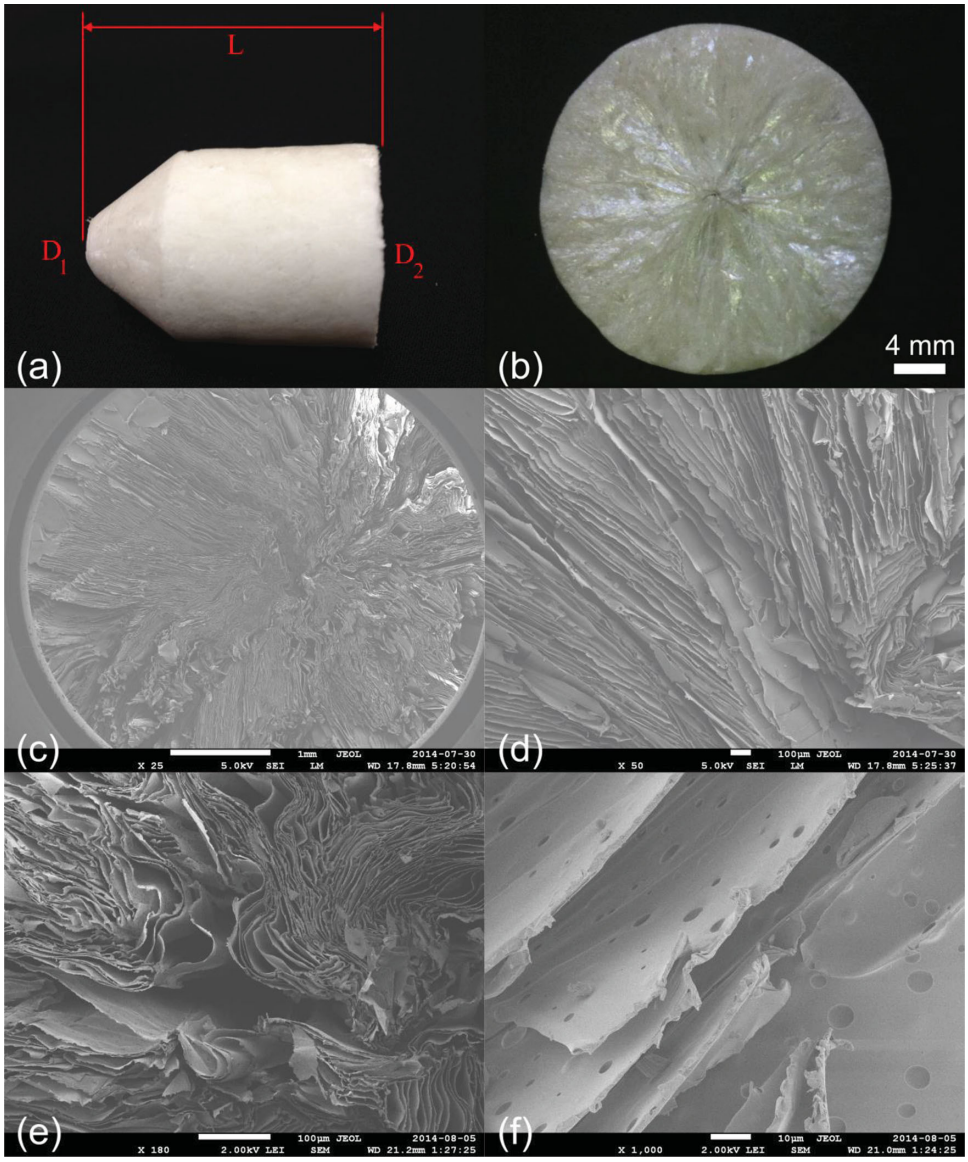

Figure 1. (a) A typical sample of a silk foam; (b) transverse cut of a silk foam sample; SEM images of the foam crossection taken with different magnifications in the vicinity of the sample center: (c) large scale view, (d) vicinity of the center, (e,f) exactly at the center.

Table 1. Porosity of the silk bulk foams.

	0	1	2	3
				
Weight [g]	0.989	0.753	0.500	0.360
L [mm]	34.0	27.7	21.0	16.8
D_2 [mm]	24.0	23.8	23.6	23.5
Filling factor [$V_{fibroin}/V_{sample}$]		5.0%	5.8%	6.4%

*D_1 = 6.9 mm (see Figure 1a)

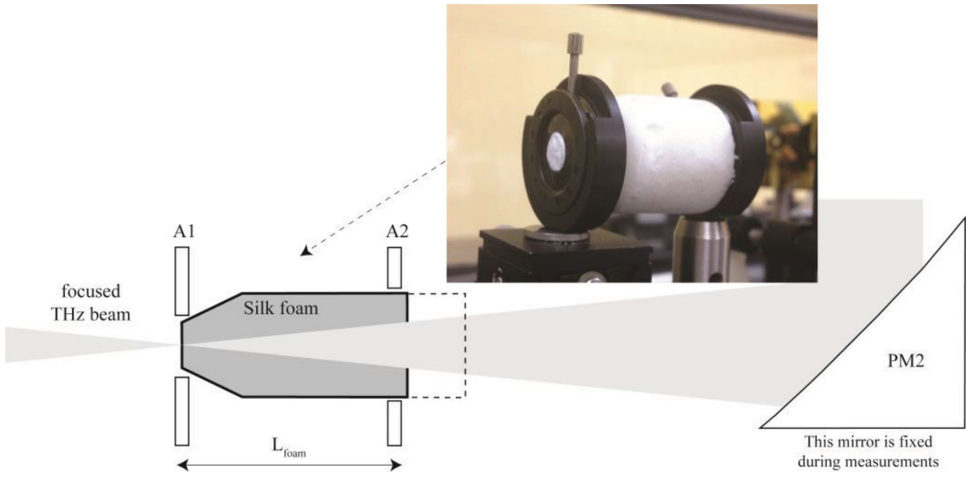

Figure 2. Schematic of the THz setup used for characterization of the bulk foam samples.

was used to collect the transmitted light. The focal point of the second parabolic mirror was aligned with that of the first parabolic mirror (and the center of the aperture) during all experiments. As the size of the collimated beam produced by the THz emitter is ~1–2 cm diameter, and because of the relatively long focal lengths of the two parabolic mirrors, we consider that propagation of light in a focused THz beam is virtually parallel to the sample symmetry axis. Finally, cutback measurements were performed on the two samples by cutting several pieces from each sample and measuring the transmission through the remaining material. The results of these measurements are presented in **Figure 3**(a) (transmission spectra) and in **Figure 4** (time traces). Time traces were obtained by averaging over 20, 200 ps-long THz traces. A typical signal-to-noise ratio in our measurements was ~20 dB.

2.3. Interpretation of the Cutback Measurements

2.3.1. Spectral and Phase Analysis of the Cutback Data

The real part of the foam effective refractive index $n^r_{foam}(\omega)$ and the foam extinction coefficient $\alpha_{foam}(\omega)$ were extracted from the measured cutback data using standard data fitting approach detailed elsewhere (see refs. [31,32], for example). In our analysis we neglect multiple reflections within the sample (Fabry-Pérot effect) as spectral intensity oscillations associated with this effect are not discernible in the measured data. The complex field transmission coefficient through the sample is then given by:

$$\frac{E_{foam}}{E_{ref}} = t(\omega)e^{i\varphi(\omega)}$$
$$t(\omega) = t_0 \exp\left(-\alpha(\omega)L_{foam}\right); t_0 = \frac{4n^r_{foam}(\omega)}{\left(n^r_{foam}(\omega)+1\right)^2} \quad (1)$$
$$\varphi(\omega) = \varphi_{foam}(\omega) - \varphi_{ref}(\omega) = -\frac{\omega}{c}(n^r_{foam}(\omega)-1)L_{foam}$$

where E_{foam} and E_{ref} are the complex amplitudes of the THz signal with and without a foam sample respectively, and L_{foam} is the length of the foam sample. The transmission coefficient takes into account the loss of intensity due to reflections at the two interfaces between foam and air (coefficient t_0), as well as absorption $\alpha_{foam}(\omega)$ due to propagation through a lossy foam sample. Note that in the case of foams $t_0 \approx 1$ as the foam refractive index is close to 1. Since the complex amplitude could be obtained directly from the THz-TDS measurements, we can, therefore, measure experimentally both the field transmission coefficient $t(\omega)$, and the phase difference $\varphi(\omega)$, from which, the real part of the refractive index and the foam extinction coefficient can be calculated using expressions in (1). In Figure 3(a) we present transmission spectra as measured by the cutback method. If all the spectra are to be used in the interpretation of the cutback results, then our analysis is limited to a narrow frequency range $0.15THz < \nu < 0.45THz$, where all the spectra are above the noise level. At these relatively low frequencies, the loss extracted from the cutback data (see Figure 3(c)) can be fitted very well with a second order polynomial with respect to frequency:

$$\alpha_{foam}[cm^{-1}] \approx 0.18 + 8.25 \cdot \left(\nu[THz]\right)^2 \quad (2)$$

In fact, the quadratic scaling of absorption losses is typical for many amorphous materials in the THz range, which is caused by the disorder-induced coupling of radiation into the acoustic phonon modes of the material.[33]

In Figure 3(b) we show unwrapped phase relative to the reference (empty system). Fitting of the cutback phase data allows us to extract the effective refractive index, which is shown in Figure 3(d). At low frequencies we find that the refractive index is virtually constant and equals to:

$$n^r_{foam} \approx 1.0594 \quad (3)$$

From experimental data presented in Figure 3(d), we can also estimate the upper bound for the chromatic dispersion of the bulk foam, which is an important parameter as it allows characterization of the temporal broadening of a THz pulse after propagation over some distance in the foam. To make the estimate, we use Taylor expansion of the foam refractive

DOI: 10.1002/adom.201400228

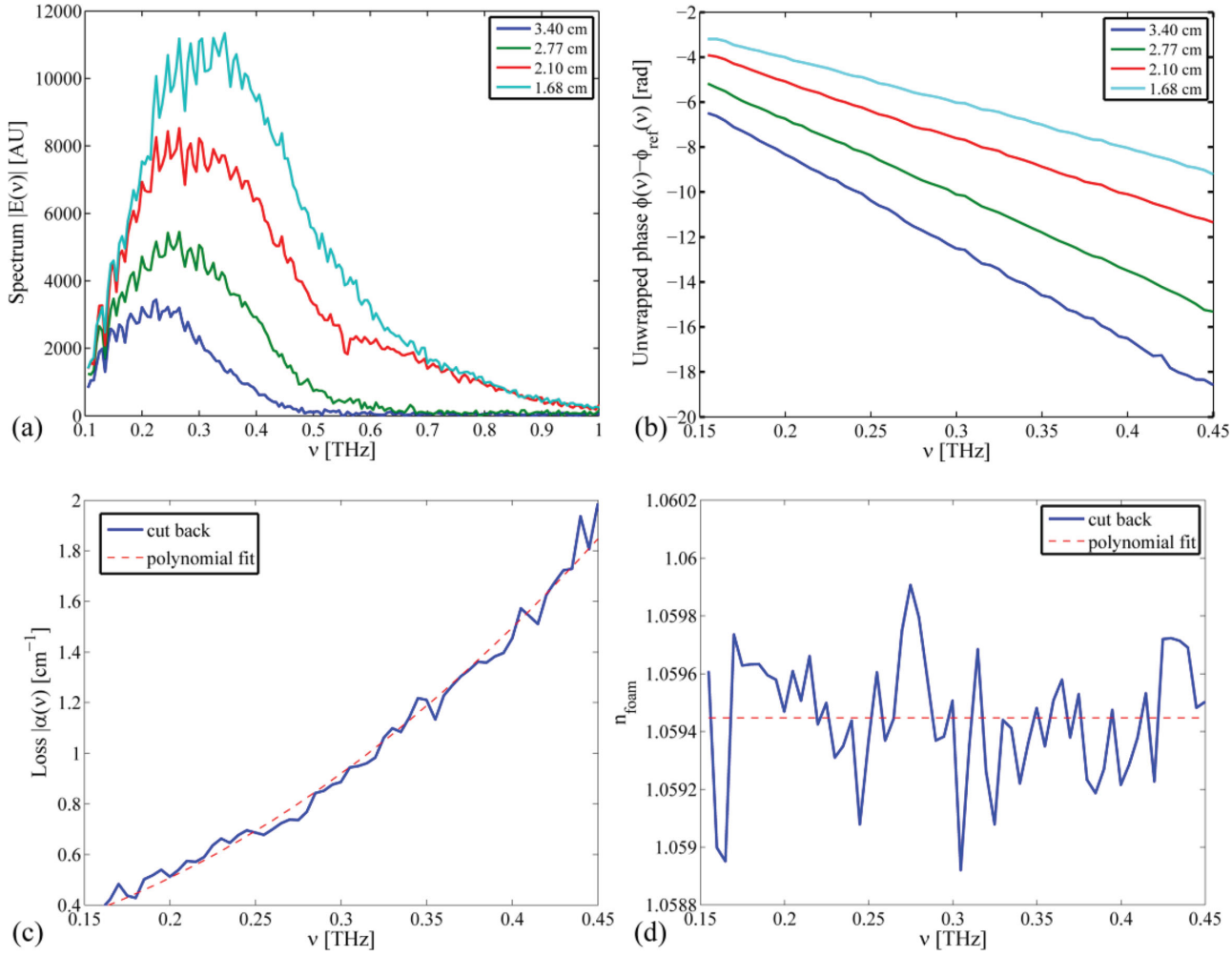

Figure 3. Cutback measurements using bulk foam sample presented in Figure 1. a) Unnormalized transmission spectra, b) unwrapped phases (relative to the reference), c) foam absorption losses, d) foam refractive index.

index in the vicinity of zero frequency, while keeping only two leading terms in order to fit the experimental data presented in Figure 3(d):

$$n^{r}_{foam}(\omega) \approx n_0 + \beta_1 \omega \tag{4}$$

From (4) and Figure 3(d) we find that $|\beta_1| < 0.0015 THz^{-1}$. The group velocity dispersion of the bulk foam is then

$$D_{foam} = \frac{\partial v_g^{-1}}{\partial \omega} = \frac{1}{c}\frac{\partial^2 \left(n^{r}_{foam}(\omega)\omega\right)}{\partial \omega^2} \approx 2\frac{\beta_1}{c} \tag{5}$$

which allows us to estimate the upper limit of the foam group velocity dispersion:

$$|D_{foam}| < 0.05 ps/(THz \cdot cm) \tag{6}$$

To put this number into perspective, this value of dispersion signifies that a 1 ps-long THz pulse will have to propagate over 20 cm in the bulk foam in order to experience 1 ps temporal broadening. This value of the material dispersion should be compared to the ~1 ps/(THz·cm) group velocity dispersion of the fundamental mode of a typical subwavelength plastic fiber, as well as ~0.002 ps/(THz·cm) group velocity dispersion of the plasmonic modes in parallel metallic plate waveguides, which are known for their outstanding guidance properties. Note also that the dispersion value (6) is only an upper bound estimate for the bulk foam dispersion, while the actual value could be significantly smaller.

2.3.2. Time Trace Analysis of the Cutback Data

We note that polynomial approximations for the foam loss (2) and for the foam refractive index (3) found from the spectral and phase analysis of the cutback data has a limited spectral region of validity. Therefore, when trying to reproduce the measured cutback time traces using (2) and (3), one does not expect to find a good agreement. Particularly, from (1) it follows that the time trace obtained during measurement of a foam sample of length L can be calculated from the reference time trace using a combination of Fourier transform and its inverse:

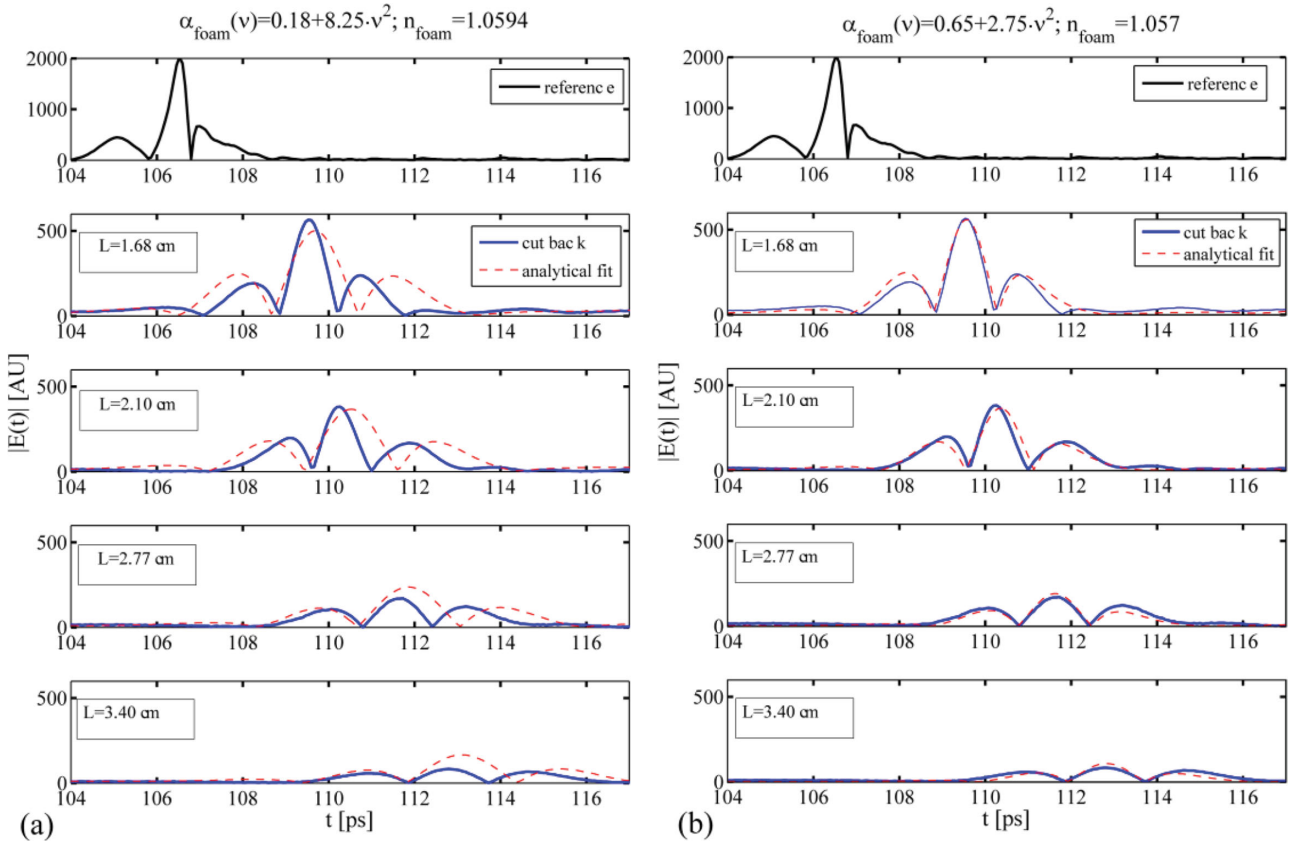

Figure 4. Time traces corresponding to the cutback measurements of a bulk foam sample of Figure 1. (a) Solid lines – experimentally measured time traces, dotted lines – analytical fit (7) using (2), (3) for the foam refractive index and bulk loses obtained by interpreting spectral transmission data at low frequencies. (b) Solid lines – experimentally measured time traces, dotted lines – analytical fit (7) using (9), (10) for the foam refractive index and bulk losses obtained by minimizing the difference between experimental and theoretical time traces.

$$E_{foam}(t, L_{foam}) \approx ifft\left(fft\left(E_{ref}(t)\right) e^{-i\frac{\omega}{c}(n^r_{foam}(\omega)-1)L-\alpha_{foam}(\omega)L} \right) \quad (7)$$

In order to use (7) one has to know frequency dependence of the foam refractive index and its losses in the whole THz spectral range. However, polynomial approximations (2), (3) were found by fitting experimental data only at low frequencies $0.15THz < \nu < 0.45THz$. Therefore, it is not surprising that using (7) together with (2) and (3) does not result in good correspondence between the measured and predicted time traces (see Figure 4(a)). Nevertheless, cut-back measurements are still useful as they provide a consistency check for the values of the foam loss and the foam refractive index, albeit in a limited spectral range.

In order to improve the fit of the pulse traces, we again assume frequency independent foam refractive index n^r_{foam}, as well $\alpha_{foam} = \alpha_0 + \alpha_1 \cdot \nu^2$ dependence of the foam losses on frequency. Next, we adjust the values of n^r_{foam}, α_0 and α_1 in order to obtain the best possible fit between the experimental and analytical results. Particularly, we note that n^r_{foam} mostly effects pulse position along the time axis, α_1 has a strong effect on the pulse width, while α_0 mostly effects pulse amplitude. In Figure 4 we plot absolute value of the electric field, which is convenient when fitting pulse bandwidth and pulse positions as zeroes, maxima and minima of the electric field are easily identifiable in this case. Therefore, by fitting the pulse positions, the pulse widths and the pulse relative amplitudes we can fit very well all the pulse traces assuming the following bulk properties of the silk foams:

$$\alpha_{foam}[cm^{-1}] = 0.65 + 2.75 \cdot \left(\nu[THz]\right)^2 \quad (8)$$

$$n^r_{foam} = 1.057 \quad (9)$$

We note that due to high content of the low-loss dry air in silk foam, the foam bulk absorption is significantly smaller than that of a solid silk. Particularly, from (2) and (9) we conclude that at 0.3THz foam absorption loss is ~0.9 cm^{-1}, while that of solid silk is ~15 cm^{-1}. Therefore, the use of silk foams can significantly expand the usefulness of this important bio-friendly material in the THz spectral range due to the foam reduced absorption losses.

3. Silk Fiber Measurement

Encouraged by the relatively low losses of silk foams, we then studied the possibility of THz guidance using silk foam-based fibers. The fibers were cast from the purified silk solution using straw molds and lyophilisation technique, thus allowing us to fabricate ~10 cm-long silk fibers of 5 mm diameter.

Adv. Optical Mater. 2014,
DOI: 10.1002/adom.201400228

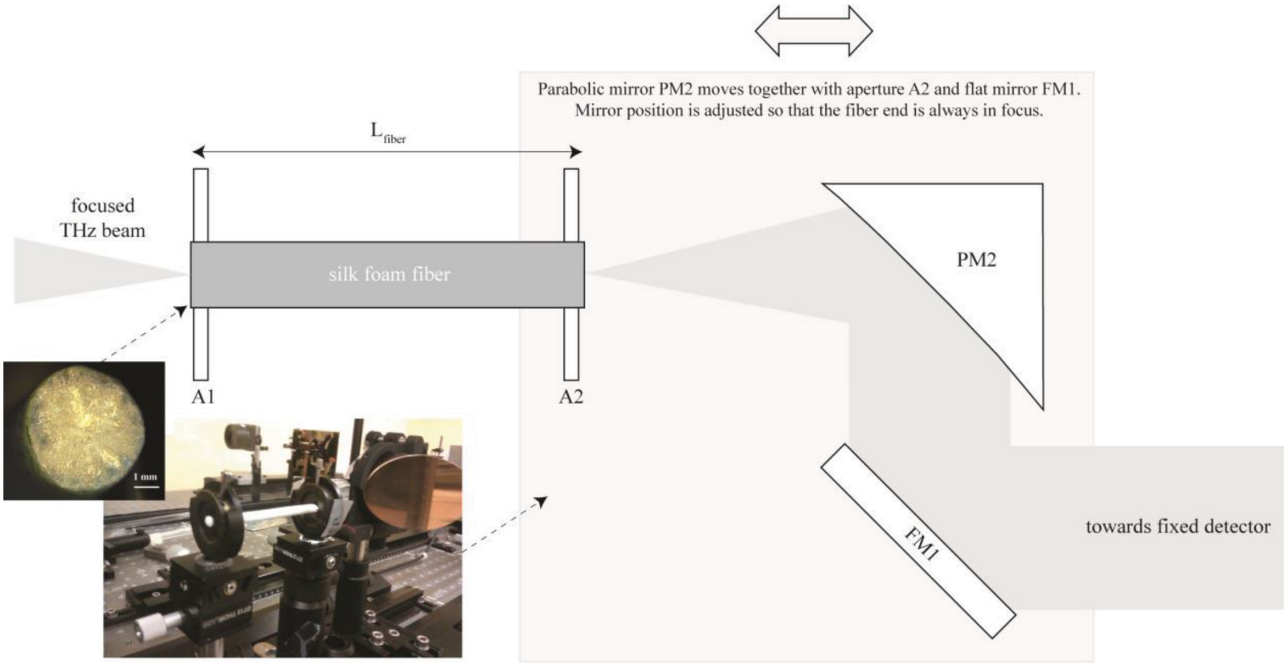

Figure 5. Schematic of the THz setup used for characterization of the foam-based fibers. Inserts – 5 mm-diameter fiber crossection, silk foam fiber mounted inside of a setup.

3.1. Optical Characterization of the Silk Foam Fibers in the THz Spectral Range

The cutback method was used in order to measure fiber propagation loss and modal effective refractive index. In **Figure 5** we present schematic of the setup used in our experiments, while in the insets we show a photo of the 5 mm-diameter fiber mounted inside the setup, as well as fiber crossection. In contrast to the case of bulk foam samples presented in the previous sections, transverse structure of the foam fibers is considerably more uniform, which is clearly related to the difference in dynamics of the lyophilisation process. While the micro-sized crystalline silk domains are still visible on the photographs of fiber crossections as speckles of colored light, at the same time, a clearly defined pattern of radially aligned domains (as seen in Figure 1(c–f)) is missing in the case of fibers. For optical characterization, the fibers were held straight and aligned with respect to the apertures A1 and A2 that marked the locations of the focal points of the input and output off-axis parabolic mirrors (see Figure 5). Reliable and efficient coupling between the THz beam and the fiber was easy to realize as the fiber diameter is somewhat larger than the THz beam diameter of 3 mm.

3.2. Interpretation of the Cutback Measurements of Silk Foam Fibers

3.2.1. Spectral and Phase Analysis of the Cutback Data

The modal transmission characteristics are deduced from the cutback data and fitting procedure describe in the literature.[31,34] In general, the normalized transmission through the fiber is given by:

$$\frac{E_{mode}(\omega,L)}{E_{ref}(\omega)} = C_{in}(\omega)C_{out}(\omega)e^{i\varphi(\omega)}\cdot e^{-\alpha_{mode}(\omega)L}$$
$$\varphi(\omega) = -\frac{\omega}{c}\left(n_{mode}(\omega)-1\right)L \quad (10)$$

where E_{mode} is the complex electric field of the propagating mode characterized by the effective refractive index $n_{mode}(\omega)$ and propagation loss $\alpha_{mode}(\omega)$. L is the fiber length, E_{ref} is the reference electric field measured without fiber at the position of the coupling plane, while $C_{in}(\omega)$ and $C_{out}(\omega)$ are the frequency dependent input and output coupling coefficients. Fiber transmission spectra are presented in **Figure 6**(a) for four different fiber lengths. If all the spectra are to be used in the interpretation of the cutback results, then our analysis has to be limited to a narrow frequency range $0.2THz < \nu < 0.4THz$, where intensities of all the spectra are above the noise level. At these frequencies, the loss extracted from the cutback data (see Figure 6(c)) can be fitted well with a second order polynomial with respect to frequency:

$$\alpha_{mode}[cm^{-1}] \approx 0.035 + 3.1\cdot\left(\nu[THz]\right)^2 \quad (11)$$

At higher frequencies, due to modal confinement of the fundamental mode in the fiber core, modal propagation loss is expected to follow closely absorption loss of the core material (silk foam) $\alpha_{mode} \approx \alpha_{foam}$. At lower frequencies, modal propagation loss can be, in principle, significantly lower than the foam absorption loss as modal fields have significant presence outside of the fiber core and in the low-loss gaseous cladding. In practice, consistent measurements at lower frequencies are problematic as fiber modes become sensitive to the core surface roughness and various environmental factors that change during sample handling.

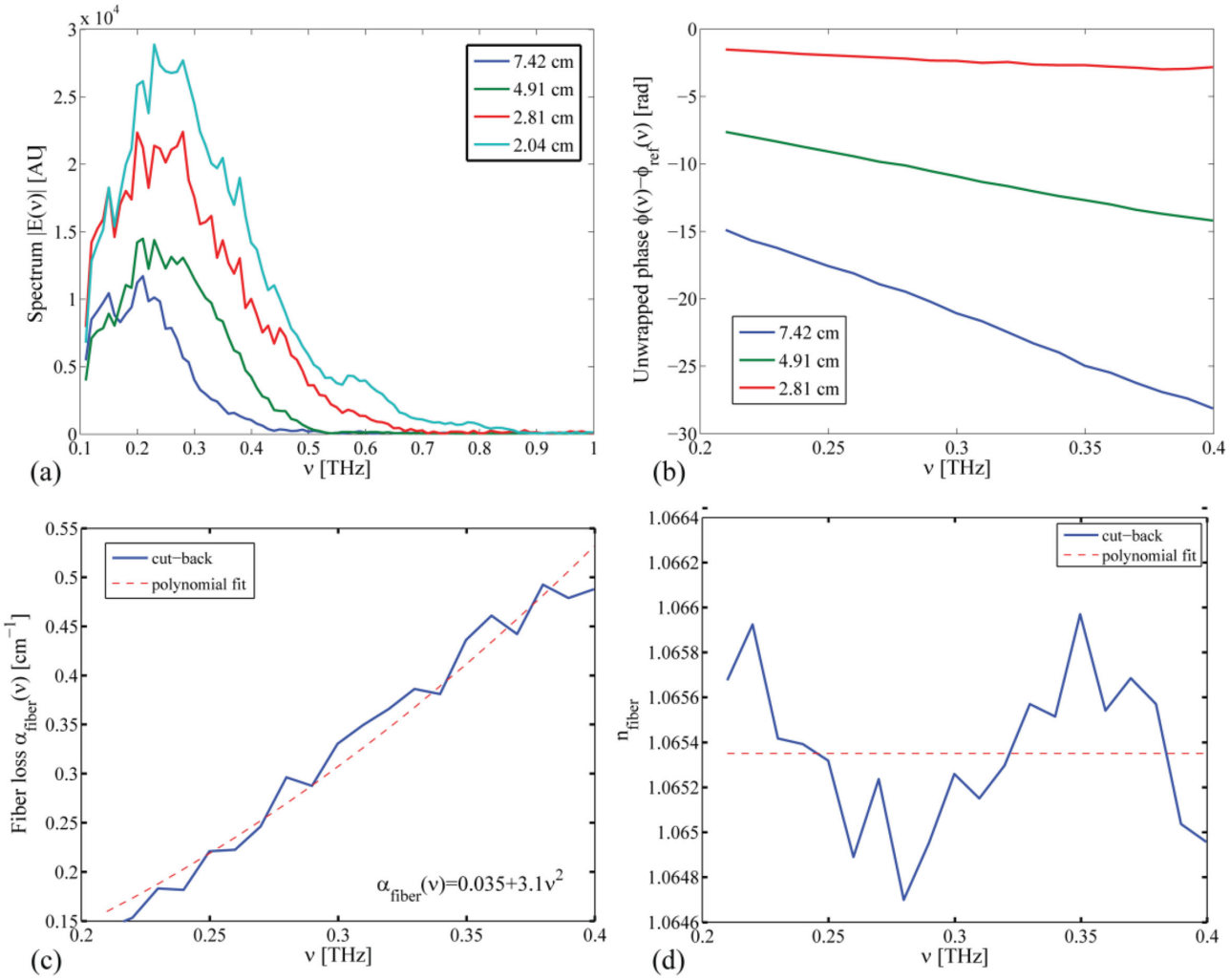

Figure 6. Cutback measurements using 5 mm-diameter silk foam fiber. a) Unnormalized transmission spectra, b) unwrapped phases (relative to the 2.04 cm-long fiber reference). Extracted c) fiber absorption losses, d) modal effective refractive index.

In order to extract phase information we use as a reference transmission data for the shortest fiber of length $L_0 = 2.04cm$. In this case, from (10) it follows that the normalized transmission through the fiber of length L can be presented as:

$$\frac{E_{mode}(\omega, L)}{E_{mode}(\omega, L_0)} = e^{i\varphi(\omega)} \cdot e^{-\alpha_{mode}(\omega)(L-L_0)} \quad \varphi(\omega) = -\frac{\omega}{c}\left(n_{mode}(\omega) - 1\right)(L - L_0) \tag{12}$$

Using the complex normalized transmission spectra (12), we can then extract modal phase information for different fiber lengths (see Figure 6(b)). Extraction of the modal effective refractive index from the unwrapped phase data can be somewhat problematic in the case of guided modes at low frequencies ($\nu < 0.2THz$ as defined in the next section). This is related to the fact that at low frequencies, the intensity of THz source is weak and the data is prone to noise; additionally, modal refractive index vary significantly at low frequencies due to rapid changes in the modal confinement. At higher frequencies, fundamental mode effective refractive index becomes virtually constant and is close to the refractive index of the core material (silk foam). Considering that in the frequency region $0.2THz < \nu < 0.4THz$, modal effective refractive index is constant, analysis of the phase data (see Figure 6(d)) gives the following value for the effective refractive index of the core mode:

$$n^r_{mode} \underset{\nu > 0.2THz}{\approx} 1.0654 \tag{13}$$

3.2.2. Time Trace Analysis of the Cutback Data

A complementary method of finding the modal propagation characteristics is to fit directly the measured cutback time traces. In what follows we use as a reference the time trace $E_{fiber}(t, L_0)$ corresponding to the shortest fiber piece L_0. Then, the time trace corresponding to the fiber of length $L > L_0$ can be calculated as:

$$E_{fiber}(t, L) \approx ifft\left(fft\left(E_{fiber}(t, L_0)\right) e^{-i\frac{\omega}{c}(n^r_{mode}(\omega)-1)(L-L_0) - \alpha_{mode}(\omega)(L-L_0)} \right) \tag{14}$$

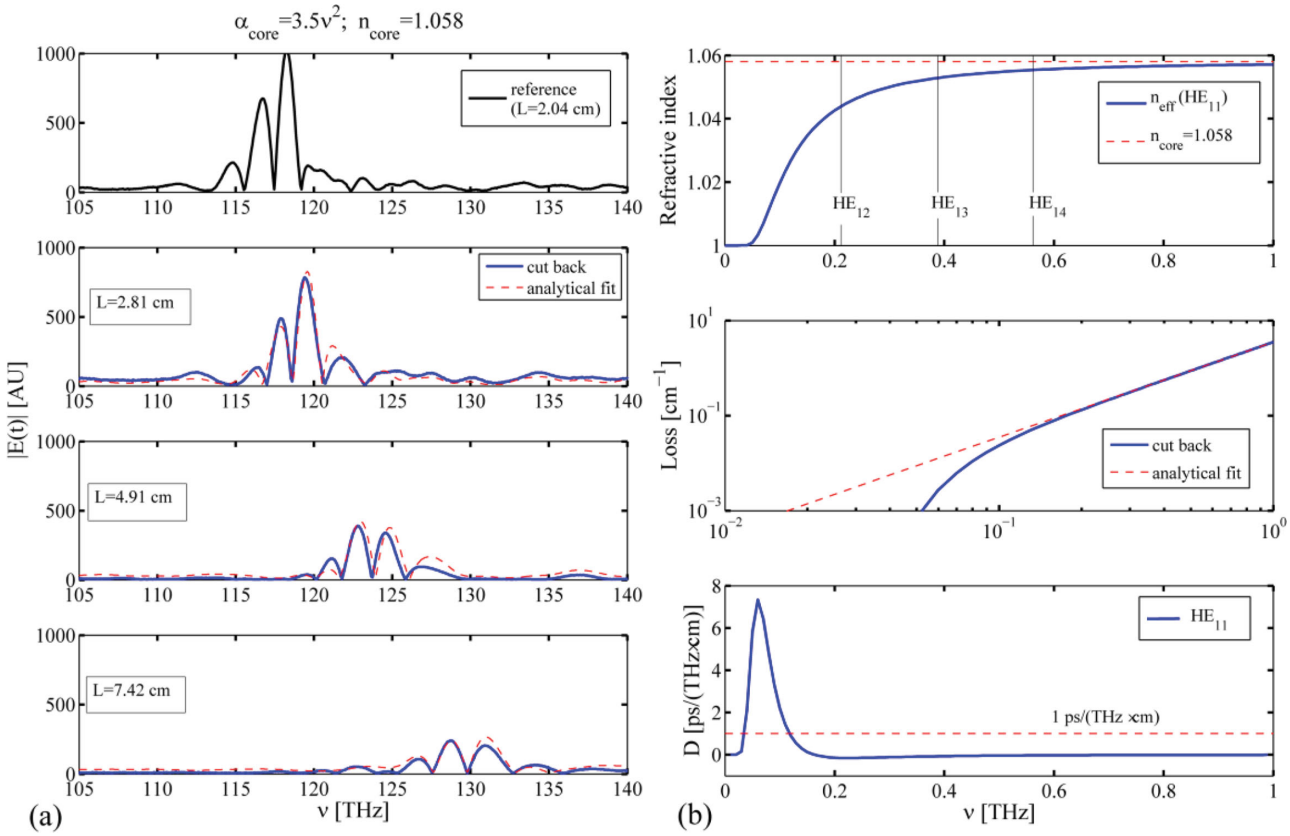

Figure 7. Time traces corresponding to the cutback measurements of 5 mm-diameter silk foam fibers. (a) Solid lines – experimentally measured time traces, dotted lines – analytical fit (14) using (15), (16) for the core material refractive index and bulk losses. (b) Optical properties of the fundamental HE_{11} mode of a silk foam fiber.

In order to reproduce reliably the time traces at various fiber lengths using (14), one needs to know the dependence of the modal refractive index (real part), as well as of the modal losses in a broad frequency range covering the whole THz spectrum. Polynomial approximations for the modal loss (11) and for the modal effective refractive index (13) found from the spectral and phase analysis of the cutback data are only valid in the narrow spectral range of $0.2THz < \nu < 0.4THz$. Therefore, when trying to reproduce the measured cutback time traces using (11) and (12), one does not, generally, expects to find a good agreement. In order to approximate correctly modal refractive index and modal loss in the broad THz frequency range, we evaluate them from the exact complex dispersion relation of the fundamental HE_{11} mode of a 5 mm-diameter circular step-index fiber. This dispersion relation is calculated using standard transfer matrix theory (see, for example[35] assuming silk foam as a core material. Particularly, we suppose that the real part of the core refractive index is frequency independent n^r_{core}, while the core material absorption losses have quadratic dependence on frequency $\alpha_{core} = \alpha_1 \cdot \nu^2$. Next, we adjust the values of n^r_{core} and α_1 in order to obtain the best possible fit between the experimental and analytical time traces. Particularly, for every choice of the core material parameters n^r_{core}, α_1 we recalculate the fundamental HE_{11} mode dispersion relation that we later use in (14) to compute the time traces. As in the case of bulk foam samples, we note that n^r_{core} mostly effects pulse position along the time axis, while α_1 has a strong effect on the pulse width. By fitting the pulse positions and the pulse widths for various fiber lengths (see **Figure 7**(a)), we find the following core material parameters that best fit all the time traces:

$$\alpha_{core}[cm^{-1}] = 3.5 \cdot \left(\nu[THz]\right)^2 \tag{15}$$

$$n^r_{core} = 1.058 \tag{16}$$

The found values for the core material refractive index and losses are close to the values found for the bulk foam samples (9), (10). For completeness, in Figure 7(b) we present dispersion relation and losses of the fundamental HE_{11} mode of a 5 mm-diameter silk foam fiber calculated using core material parameters (15), (16).

4. Guidance Mechanism in the Silk Foam Fibers

As it is detailed in our prior work,[24,31,35] a circular microporous step-index fiber operates in the subwavelength regime if the operation frequency is smaller than a characteristic value of $\nu_0 = c/\left(\pi d\sqrt{\Delta\varepsilon}\right)$ (see p. 116, and ch. 11 of ref. [35]), where d is the fiber diameter and $\Delta\varepsilon$ is the difference in the effective dielectric constants of the fiber core and cladding materials. In the case of

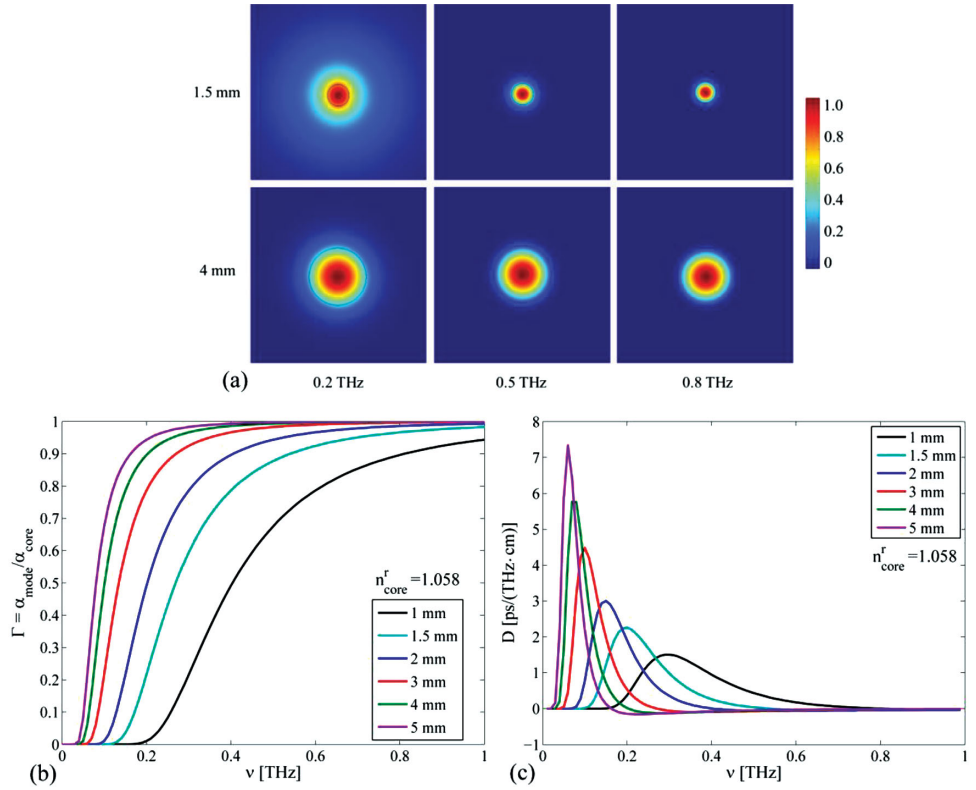

Figure 8. (a) Longitudinal flux distribution in the fundamental HE_{11} mode of a step-index silk foam fiber at various frequencies. Black circle marks the core/cladding interface. Top row – fiber diameter is 1.5 mm. Bottom row – fiber diameter is 4.0 mm. (b) Propagation loss of HE_{11} mode normalized by the bulk absorption loss of the core material. c) Group velocity dispersion of the HE_{11} mode.

silk foam fibers considered in this work ($d \sim 5\ mm, n_{core} \sim 1.058$), the characteristic frequency is, therefore, $\nu_0 \sim 0.055 THz$. In the subwavelength guidance regime the fiber supports a single doubly degenerate HE_{11} mode, which has a strong field presence outside of the fiber core. In this regime, modal guidance is very sensitive to the environment, and light guidance can be easily lost due to scattering on the imperfections at the core/air interface. In the vicinity of ν_0, the fundamental mode shows fast transition from the subwavelength guidance regime to the strong confinement in the fiber core (see Figure 7(b)), thus resulting in the relatively large value of the modal group dispersion $D_{\max}\underset{\nu\sim\nu_0}{\sim} d\Delta\varepsilon^{3/2}/\left(4c^2 n_{clad}\right) \approx 6\, ps/(THz\cdot cm)$. When increasing operation frequency, the mode remains well confined in the fiber core, and eventually, at frequencies higher than $2.41\cdot\nu_0 \sim 0.13 THz$ the fiber becomes multimode. For practical purposes, however, the multimode nature of the fiber does not reveal itself up to a higher frequency of $3.83\cdot\nu_0 \sim 0.21 THz$ (see p. 121 of ref. [35]), as centered and normally incident THz Gaussian beam used for fiber excitation cannot excite most of the higher order modes due to symmetry mismatch. At these intermediate frequencies fiber mode dispersion decreases to a fraction of its maximal value (achieved in the vicinity of ν_0), and it becomes smaller than $\sim 1 ps/(THz\cdot cm)$ (see Figure 7(b)). Furthermore, even at frequencies as high as $10.2\cdot\nu_0 \sim 0.56 THz$, only 4 modes can be excited in the fiber core (using THz Gaussian beam focused into the fiber center as the excitation source), with most power propagating in the fundamental HE_{11} mode. Finally, at these higher frequencies, modal loss is virtually identical to the bulk absorption loss of the silk foam due to high modal confinement in the fiber core.

In **Figure 8** we summarize some important properties of the fundamental HE_{11} mode of silk foam fibers of various diameters. We assume the core refractive index to be $n^r_{core} = 1.058$. In Figure 8(a) we present the longitudinal flux distributions corresponding to the fundamental HE_{11} modes of the two silk fibers with diameters of 1.5 mm and 4 mm at various operation frequencies. At low frequency (0.2 THz), a significant portion of the modal fields is found outside of the fiber core and in the low-loss air cladding, which is especially pronounced for the 1.5 mm-diameter fiber. This is the regime of subwavelength guidance. When increasing the frequency of operation significantly beyond the characteristic frequency of subwavelength guidance ($\nu_0 \sim 0.06 THz$ for 4mm-diameter fiber and $\nu_0 \sim 0.16 THz$ for a 1.5 mm-diameter fiber), the fundamental guided mode shows strong localisation in the fiber core. In this regime, fiber propagation loss becomes virtually identical to the core material loss. In Figure 8(b) we present loss of the fundamental fiber mode normalised by the value of the core material absorption loss $\Gamma = \alpha_{mode}/\alpha_{core}$. Clearly, transition from the subwavelength guidance regime to the regime of strong confinement of the modal fields in the fiber core clearly correlates with the rapid increase in the modal propagation loss.

Finally, in Figure 8(c) we present group velocity dispersion of the fundamental mode of a foam fiber for various values of the fiber diameter. Modal dispersion is maximal in the vicinity of the characteristic frequency ν_0 which is not surprising as modal

Adv. Optical Mater. 2014,
DOI: 10.1002/adom.201400228

localization changes rapidly in this frequency range. In the regime of strong modal confinement in the fiber core ($\nu > \nu_0$), modal dispersion is significantly lower than its maximal value by as much as two orders of magnitude. Therefore, for larger diameter fibers (>3 mm), at frequencies above 0.2 THz, modal dispersion is can be significantly lower than $1ps/(THz \cdot cm)$. At the same time, modal losses will be identical to that of the core material, which can become significant at higher frequencies ($> 3cm^{-1}$ at 1 THz). For smaller diameter fibers (<3 mm), the characteristic frequency ν_0 shifts into the mid THz range and group velocity dispersion becomes significant $> 1ps/(THz \cdot cm)$ even at higher frequencies >0.2 THz. At the same time, in mid-THz frequency range, small diameter fibers guide predominantly in the subwavelength guidance regime characterized by small propagation losses $< 1cm^{-1}$ at 1 THz. Therefore, when deciding on the optimal diameter of a foam fiber, there is a tradeoff between high loss/low modal dispersion of the large-core fibers and low loss/high modal dispersion of the small-core fibers.

5. Discussion

We would like to comment now on several important properties of silk foams and waveguides made from such foams that were demonstrated in this paper. First, the absorption loss of silk foams in THz spectral range is reduced by almost one order of magnitude compared to that of the bulk silk. By further decreasing the porosity of the silk foam, we could further reduce the foam loss to be comparable to that of standard low-loss THz plastics such as polyethylene. At the same time, the main advantage of the silk foam compared to standard plastics is that it is biocompatible, biodegradable and, due to its porous nature, it could be biofunctionalized with various materials. Moreover, the foam porous structure can be useful for sampling of various biofluids using capillary effect for applications in biosensing, for instance. This cannot be done with standard plastics. On the other hand, if the goal is to prevent liquid penetration in the liquid core, one can trivially seal the pores on the fiber surface.

Second, in this paper we report a waveguide that has air as cladding, and therefore the guided mode is partially present outside of the foam material. In order to confine the guided mode fully within the fiber structure one can use foams of two different densities for the fiber core and cladding regions. As it follows from the discussion of the theoretical section, foam based fibers can be designed with 1-mm dimensions, thus making it comparable with many existing endoscopes for in vivo applications.

Finally, we want to clearly distinguish foam fibers presented in this paper and porous plastic fibers (see refs. [31,36], for example) developed for guidance of THz waves. The size of the pores in foams is at least an order of magnitudes smaller than the size of the pores in the abovementioned porous plastic fibers. The porous fibers are manufactured using drawing of structured preforms, therefore limiting the material of a fiber to thermoplastics. At the same time, silk cannot be drawn, therefore a completely different processing has to be used for the fabrication of silk fibers. In fact, the fabrication method presented in this paper is suitable for many biologically important water soluble materials that cannot be otherwise drawn into optical fibers. Finally, we note that although many other low-loss hollow-core terahertz waveguides exist with approximately the same fiber diameter that our silk fiber, most of such fibers are either made of plastic or plastic/metal combinations. So far, to the best of our knowledge, there were no demonstrations of THz fibers made from truly biocompatible materials such as silk.

6. Conclusion

Our work is motivated by the lack of bio-friendly waveguides for low-loss, low-dispersion guidance of terahertz waves. Such waveguides are desirable in the numerous potential applications in remote and stand-off sensing in bio-medical and agro-alimentary industries. In this paper, we present novel silk foam material that was developed in our group using freeze drying (lyophilisation) of the purified silk solutions. Weight and volume measurements show that our foam material is ~94% porous by volume. We use cutback technique to characterize optical properties of the silk foams in the THz spectral range. We find that refractive index of silk foams used in our experiments is close to that of air (~1.06), while material absorption loss of the silk foams is almost an order of magnitude smaller than that of bulk silk at THz frequencies, which is due to presence of low-loss gas in the foam structure. Moreover, bulk foam losses are strongly dependent on frequency and are in the ~1–2 cm^{-1} range at 0.5 THz, while being less than ~1 cm^{-1} at lower frequencies <0.3 THz. To demonstrate potential of silk foams for guiding of THz waves, we then cast 5 mm-diameter, 10 cm-long silk foam fibers and use cut back technique to describe their optical properties in the THz frequency range. We find that 5 mm-diameter, 10 cm-long fibers guide well in the mid THz frequency range of 0.2–0.5 THz with a typical loss less than 0.8 cm^{-1}. In this spectral range, modal group velocity dispersion is estimated to be less than $0.2ps/(THz \cdot cm)$. Our experiments confirm the overall feasibility of using silk foams as an enabling material for the development of biocompatible guided wave devices in THz frequency range.

7. Experimental Section

Purified Aqueous Silk Fibroin Solution: Bombyx mori silk is composed of silk fibroin protein covered by sericin protein. For biomedical applications, sericin should be removed as it provokes adverse reaction of the immune system.[1] Once sericin is removed, the silk fibroin protein can be dissolved in an aqueous LiBr solution, purified and then formed into various shapes using standard solution-based processes.[32] First, the Bombyx mori cocoons were cut into pieces and boiled for 30 min in a Na_2CO_3 solution (0.02 M). Then, they were rinsed three times with deionized water (20 min per rinse) in order to remove the gluey sericin protein. The degummed silk mass was then placed in the fume hood over night to dry. Next, dry silk was dissolved in LiBr solution (9.3 M) at room temperature, yielding a 20 wt% solution. This solution was then dialyzed in deionized water using a Slide-a-Lyzer dialysis cassettes (Pierce, MWCO 3500) for 48 h. After that, the solution was centrifuged twice at 4 °C with a spinning speed of 9000 r.p.m. for 20 min. Finally we have obtained an aqueous silk solution with silk concentration of

7.0–8.0 wt%, which was determined by weighing the silk material after drying a part of the solution (see ref. [37] for more details). The final silk solution is clear with a slight tint of yellow. The silk solution is slightly more viscous than water, and it can be stored at 4 °C for at least one month.

Silk Foams and Foam-Based Fibers: In order to fabricate silk foam, we used lyophilisation method that causes less damage, shrinkage or toughening of the material being dried than other dehydration methods. A conical test tube with silk solution was placed vertically in a freezer (dry ice filled box) at –80 °C for several hours until the solution was completely frozen. Then the frozen sample was connected to a low vacuum system (mechanical pump). Eventually, the water sublimated and left behind the silk foam in a test tube.

THz fibers were cast from the purified silk fibroin solution using 5 mm-diameter plastic straws as molds. We started by filling the straws with silk solution with one end of the straw connected to a syringe, while the other end immersed in solution. While filling the straws, care must be taken to avoid introduction of air bubbles. After the straws were filled, one of their ends was closed, the straws were frozen at –80 °C, and then they were placed under vacuum for lyophilisation. After the removal of water, the THz fibers were easily pushed out of the molds.

Acknowledgements

H. Guerboukha and G. Yan contributed equally to this work. This work was supported in part by the NSERC Strategic Grant 430420–12.

Received: May 15, 2014
Revised: August 13, 2014
Published online:

[1] G. H. Altman, F. Diaz, C. Jakuba, T. C. Rebecca, L. Horan, J. Chen, H. Lu, J. Richmond, D. L. Kaplan, *Biomaterials*. **2003**, *24*, 3.
[2] V. Elisseeff, *The Silk Roads: Highways of Culture and Commerce*, Berghahn Books, New York, NY, USA **2000**.
[3] S. Vainker, *Chinese Silk: A Cultural History*, Rutgers University Press, Piscataway, NJ, USA **2004**.
[4] H. Perry, A. Gopinath, D. L. Kaplan, L. D. Negro, F. G. Omenetto, *Adv. Mater.* **2008**, *20*, 16.
[5] S. T. Parker, P. Domachuk, J. Amsden, J. Bressner, J. A. Lewis, D. L. Kaplan, F. G. Omenetto, *Adv. Mater.* **2009**, *21*, 23.
[6] A. K. Manocchi, P. Domachuk, F. G. Omenetto, H. Yi, *Biotechnol. Bioeng.* **2009**, *103*, 4.
[7] R. Capelli, J. J. Amsden, G. Generali, S. Toffanin, V. Benfenati, M. Muccini, D. L. Kaplan, F. G. Omenetto, R. Zamboni, *Org. Electron.* **2011**, *12*, 7.
[8] K. Tsioris, W. K. Raja, E. M. Pritchard, B. Panilaitis, D. L. Kaplan, F. G. Omenetto, *Adv. Funct. Mater.* **2012**, *22*, 2.
[9] D.-H. Kim, J. Viventi, J. J. Amsden, J. Xiao, L. Vigeland, Y.-S. Kim, J. A. Blanco, B. Panilaitis, E. S. Frechette, D. Contreras, D. L. Kaplan, F. G. Omenetto, Y. Huang, K.-C. Hwang, M. R. Zakin, B. Litt, J. A. Rogers, *Nat. Mater.* **2010**, *9*, 6.
[10] D.-H. Kim, Y.-S. Kim, J. Amsden, B. Panilaitis, D. L. Kaplan, F. G. Omenetto, M. R. Zakin, J. A. Rogers, *Appl. Phys. Lett.* **2009**, *95*, 13.
[11] B. D. Lawrence, J. K. Marchantb, M. A. Pindrusa, F. G. Omenettoa, D. L. Kaplan, *Biomaterials* **2009**, *30*, 7.
[12] H. Tao, S. M. Siebert, M. A. Brenckle, R. D. Averitt, M. Cronin-Golomb, D. L. Kaplan, F. G. Omenetto, *Appl. Phys. Lett.* **2010**, *97*, 12.
[13] C. Li, C. Vepari, H.-J. Jin, H. J. Kim, D. L. Kaplan, *Biomaterials* **2006**, *27*, 16.
[14] S. E. Wharram, X. H. Zhang, D. L. Kaplan, S. P. McCarthy, *Macromol. Biosci.* **2010**, *10*, 3.
[15] G. H. Altmana, R. L. Horana, H. H. Lua, J. Moreaua, I. Martinb, J. C. Richmondc, D. L. Kaplan, *Biomaterials* **2002**, *23*, 20.
[16] S.-J. He, R. Valluzzi, S. P. Gido, *Int. J. Biol. Macromol.* **1999**, *24*, 2.
[17] B. D. Lawrence, M. Cronin-Golomb, I. Georgakoudi, D. L. Kaplan, F. G. Omenetto, *Biomacromolecules* **2008**, *9*, 4.
[18] J. P. Mondia, J. J. Amsden, D. Lin, L. D. Negro, D. L. Kaplan, F. G. Omenetto, *Adv. Funct. Mater.* **2010**, *22*, 41.
[19] K. Tsioris, G. E. Tilburey, A. R. Murphy, P. Domachuk, D. L. Kaplan, F. G. Omenetto, *Adv. Funct. Mater.* **2010**, *20*, 7.
[20] H. Tao, J. J. Amsden, A. C. Strikwerda, K. Fan, D. L. Kaplan, X. Zhang, R. D. Averitt, F. G. Omenetto, *Adv. Mater.* **2010**, *22*, 32.
[21] H. Tao, M. A. Brenckle, M. Yang, J. Zhang, M. Liu, S. M. Siebert, R. D. Averitt, M. S. Mannoor, M. C. McAlpine, J. A. Rogers, D. L. Kaplan, F. G. Omenetto, *Adv. Mater.* **2012**, *24*, 8.
[22] R. Mendis, D. Grischkowsky, *J. Appl. Phys.* **2000**, *88*, 7.
[23] C. S. Ponseca Jr., R. Pobre, E. Estacio, N. Sarukura, A. Argyros, M. C. J. Large, M. A. van Eijkelenborg, *Opt. Lett.* **2008**, *33*, 9.
[24] B. Ung, A. Mazhorova, A. Dupuis, M. Rozé, M. Skorobogatiy, *Opt. Express* **2011**, *19*, 26.
[25] P. Cebe, X. Hu, D. L. Kaplan, E. Zhuravlev, A. Wurm, D. Arbeiter, C. Schick, *Sci. Rep.* **2013**, *3*, 1130.
[26] X. Hu, K. Shmelev, L. Sun, E. S. Gil, S. H. Park, P. Cebe, D. L. Kaplan, *Biomacromolecules* **2011**, *12*, 5.
[27] G. Zhao, M. Mors, T. Wenckebach, P. Planken, *J. Opt. Soc. Am. B* **2002**, *19*, 6.
[28] N. C. J. van der Walk, W. A. M. van der Marel, P. C. M. Planken, *Opt. Lett.* **2005**, *30*, 20.
[29] C. Roman, O. Ichim, L. Sarger, V. Vigneras, P. Mounaix, *Electron. Lett.* **2004**, *40*, 19.
[30] H. Ishikawa, Z. K. Kozo, *Structure of Silk Proteins* (Ed: N. Hojo), Shinkyo Publishing Co., Nagano, Japan **1980**, pp.209–224.
[31] A. Dupuis, A. Mazhorova, F. Desevedavy, M. Roze, M. Skorobogatiy, *Opt. Express* **2010**, *18*, 13.
[32] O. Mitrofanov, R. James, F. A. Fernández, T. K. Mavrogordatos, J. A. Harrington, *IEEE Trans. THz Sc. & Tech.* **2011**, *1*, 1.
[33] M. Naftlay, R. E. Miles in *Terahertz Frequency Detection and Identification of Materials and Objects* (Eds: R. E. Miles, X.-C. Zhang, H. Eiseile, A. Krotkus), Springer, Netherlands **2006**, pp.107–122.
[34] R. Mendis, D. Grischkowsky, *Opt. Lett.* **2001**, *26*, 11.
[35] M. Skorobogatiy, *Nanostructured and Subwavelength Waveguides: Fundamentals and Applications*, Chichester, West Sussex, UK **2012**.
[36] S. Atakaramians, S. Afshar, V. B. M. Fischer, D. Abbott , T. M. Monro, *Opt. Express* **2008**, *16*, 12.
[37] D. N. Rockwood, R. C. Preda, T. Yücel, X. Wang, M. L. Lovett, D. L. Kaplan, *Nat. Protocols*, **2011**, *6*, 10.